Electronic Supporting Information
Accelerated Rates of Proton Coupled Electron Transfer to Oxygen Deficient Polyoxovanadate-alkoxide Clusters

Shannon E. Cooney†, Eric Schreiber†, William W. Brennessel, and Ellen M. Matson*
Department of Chemistry, University of Rochester, Rochester NY 14627 USA

Supporting Information Table of Contents:

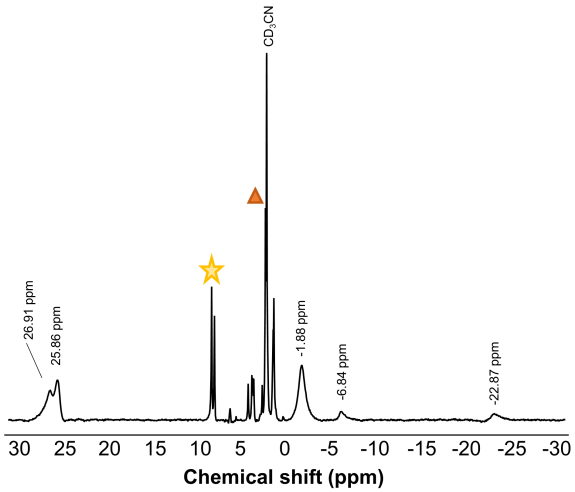

Figure S1. ^{1}H NMR spectrum of the reaction of $\mathbf{[V_6O_7]^0}$ with two equivalents of 5,10-dihydrophenazine (H_2Phen) at 294 K in CD_3CN after 3 minutes. Orange triangle represent H_2O (2.13 in CD_3CN) product and yellow star denotes phenazine.

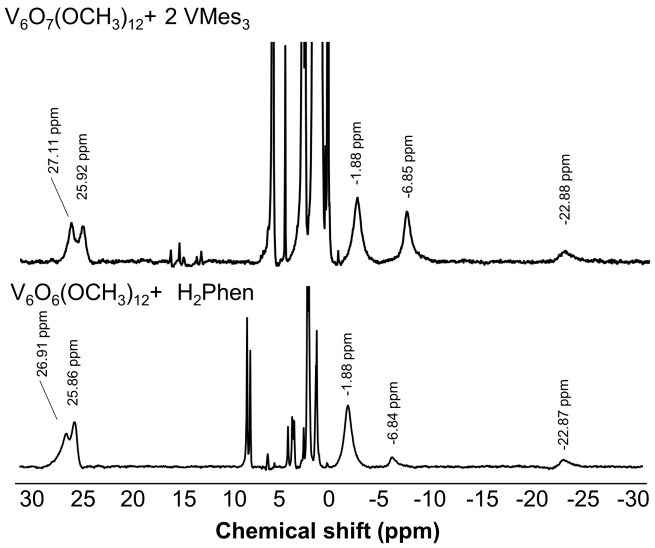

Figure S2. ^{1}H NMR spectrum of $\mathbf{[V_6O_7]^0}$ + 2 equivalents of $VMes_3$(THF) (2019, top)[1] and the synthesis of $\mathbf{[V_6O_5(MeCN)_2]^0}$ using 2 equivalents of HAT reagent (H_2Phen) (2023, bottom) at 294 K in CD_3CN.

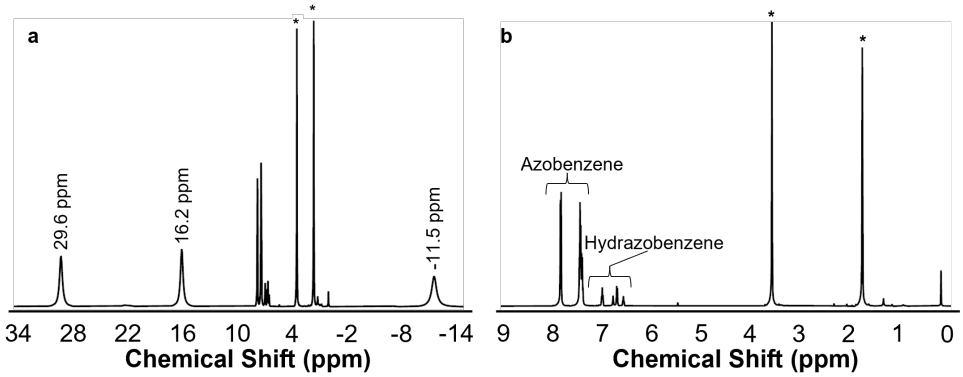

Figure S3. ^{1}H NMR spectrum of the reaction of $\mathbf{[V_6O_7]^0}$with one equivalent of hydrazobenzene (Hydz) at 294 K in THF-d_8, a- paramagnetic region showing the three peaks associated with $\mathbf{[V_6O_6(OH_2)]^0}$, b- diamagnetic region showing the formation of azobenzene and residual hydrazobenzene. Notable in this crude reaction mixture is the lack of formation of H_2O, indicating it remains bound to the cluster.

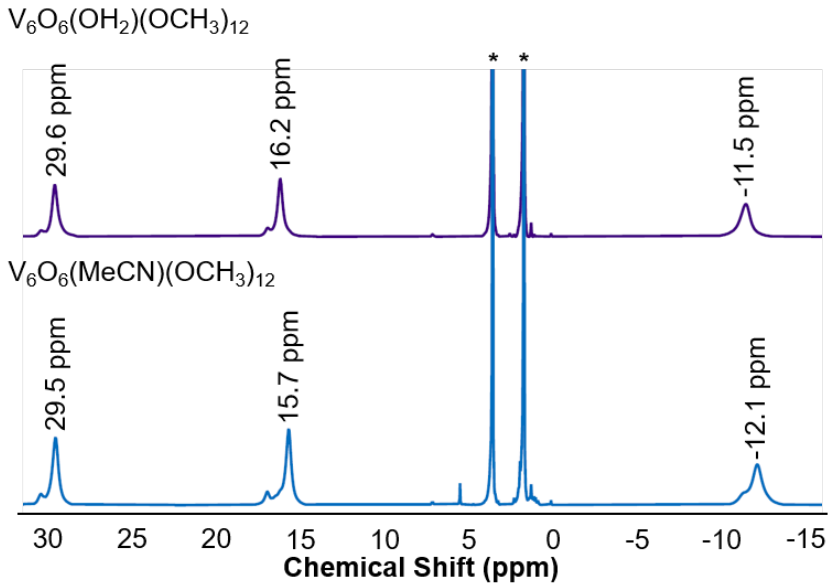

Figure S4. ^{1}H NMR spectra of $\mathbf{[V_6O_6(MeCN)]^0}$ (blue, bottom) and $\mathbf{[V_6O_6(OH_2)]^0}$ (purple, top) at 294 K in THF-d_8.

Table S1. Crystallographic parameters of the molecular structure obtained for complex **[$V_6O_6(OH_2)$]**·THF_2.

Compound	$[V_6O_6(OH_2)]\cdot THF_2$
Empirical formula	$C_{20}H_{54}O_{21}V_6$
Formula weight	936.27
Temperature / K	100.00(10)
Wavelength / Å	1.54184
Crystal group	Triclinic
Space group	*P-1*
Unit cell dimensions	a = 92190(2) Å b = 10.6059(2) Å c = 18.4535(2) Å α = 96.3890(10)° β = 90.1810(10)° γ = 91.4940(10)°
Volume / $Å^3$	1792.46(6)
Z	2
Reflections collected	54875
Independent reflections	7646
Completeness (theta)	99.4% (74.504°)
Goodness-of-fit on F^2	1.117
Final R indices [I>2sigma(I)]	R1 = 0.0360
Largest diff. peak and hole	0.535 and -0.490 e.$Å^{-3}$

Table S2. Bond valence sum calculations on the V ions of **[$V_6O_6(OH_2)$]^0**.

Oxidation State	V1[a]	V2	V3	V4	V5	V6
V^{III}	**3.067**	3.885	3.936	3.909	3.939	4.421
V^{IV}	3.141	**3.978**	**4.030**	**4.002**	**4.033**	4.526
V^{V}	3.376	4.242	4.297	4.267	4.299	**4.820**

[a] *V1 bears a terminal aquo ligand*

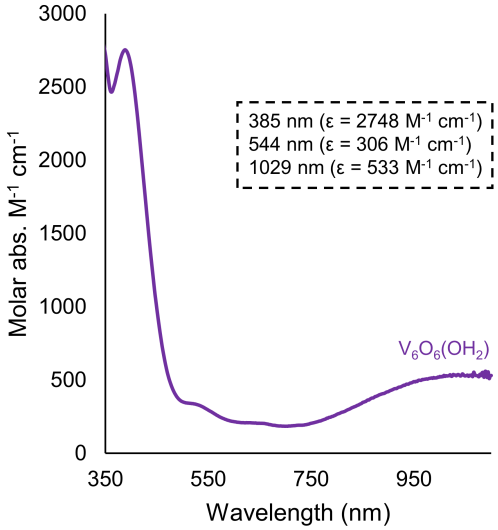

Figure S5. Electronic absorption spectrum of $[V_6O_6(OH_2)]^0$ recorded at 294 K in THF, bands are labeled in figure inset.

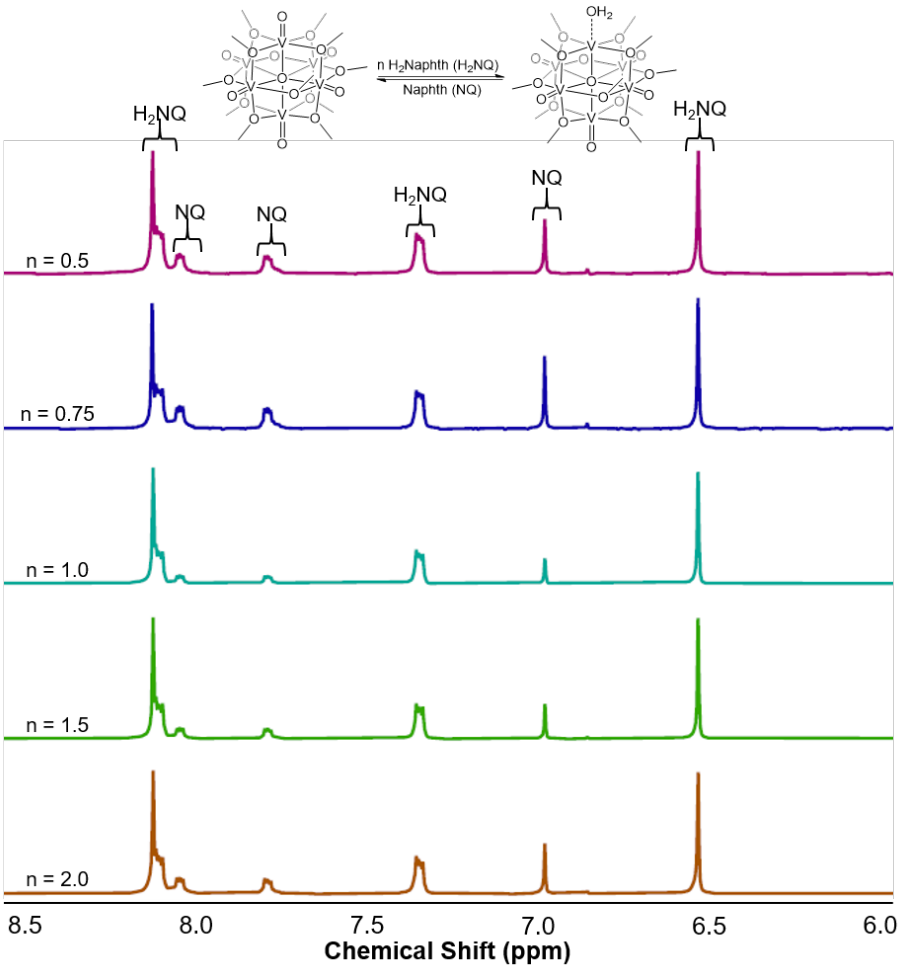

Figure S6. ^{1}H NMR spectra of reactions of 1,4-dihydroxynaphthalene (H_2Naphth) with $[V_6O_7]^0$ at various reductant:cluster ratios at 21 °C for 7 days recorded in THF-d_8 at 294 K.

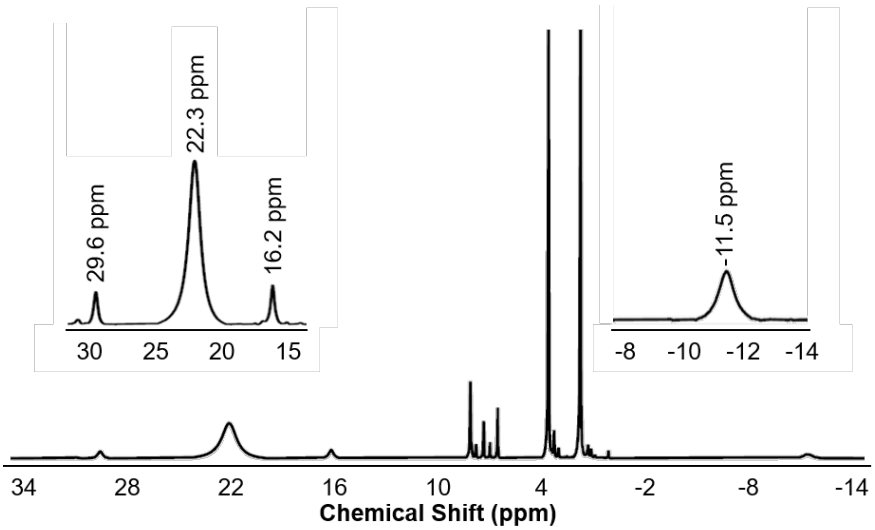

Figure S7. ^{1}H NMR spectrum of the reaction of $\mathbf{[V_6O_7]^0}$ with one equivalent of H_2Naphth at 294 K after 7 days in THF-d_8.

Table S3. $BDFE_{adj}$ calculated for $[V_6O_6(OH_2)]^0$ from equilibrium reactions described in Figure S6, using the equation outlined in the Experimental section in the main text.

	1,4-Dihydroxynaphthalene							Naphthoquinone							
	8.1 ppm (4 H)		7.3 ppm (2 H)		6.5 ppm (2 H)		Avg. Conc.	8.0 ppm (2 H)		7.8 ppm (2 H)		7.0 ppm (2 H)		Avg. Conc.	$BDFE_{adj}$ (kcal/mol)
n	Integral	Conc.[a]	Integral	Conc.[a]	Integral	Conc.[a]		Integral	Conc.[a]	Integral	Conc.[a]	Integral	Conc.[a]		
0.5	3.47	0.87	1.76	0.88	1.70	0.85	**0.87**	1.07	0.54	0.91	0.46	0.84	0.42	**0.47**	**62.4**
0.75	4.40	1.10	2.17	1.09	2.15	1.08	**1.09**	1.12	0.56	1.00	0.5	0.86	0.43	**0.50**	**62.4**
1.0	4.92	1.23	2.46	1.23	2.48	1.24	**1.23**	1.16	0.58	1.00	0.5	0.91	0.46	**0.51**	**62.3**
1.5	7.03	1.76	3.48	1.74	3.47	1.74	**1.74**	1.05	0.53	1.00	0.5	0.87	0.44	**0.49**	**62.2**
2.0	8.61	2.15	4.30	2.15	4.29	2.15	**2.15**	1.05	.525	1.00	0.5	0.88	0.44	**0.49**	**62.2**
												Avg.			**62.3**
												Std. Dev.			**0.1**

[a] Relative concentration of either 1,4-dihydroxynaphthalene or naphthoquinone was determined by dividing the integral by the number of protons a given signal(s) corresponds with.

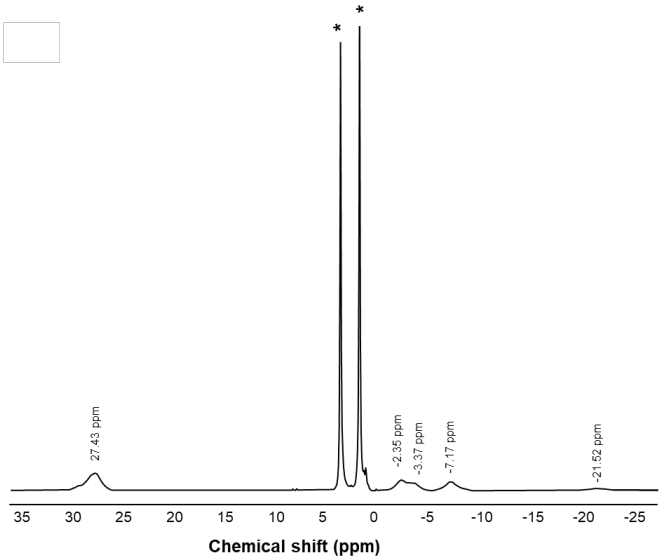

Figure S8. ^{1}H NMR spectrum of **[$V_6O_5(OH_2)(MeCN)]^0$** at 294 K in THF-d_8 (indicated by asterisks).

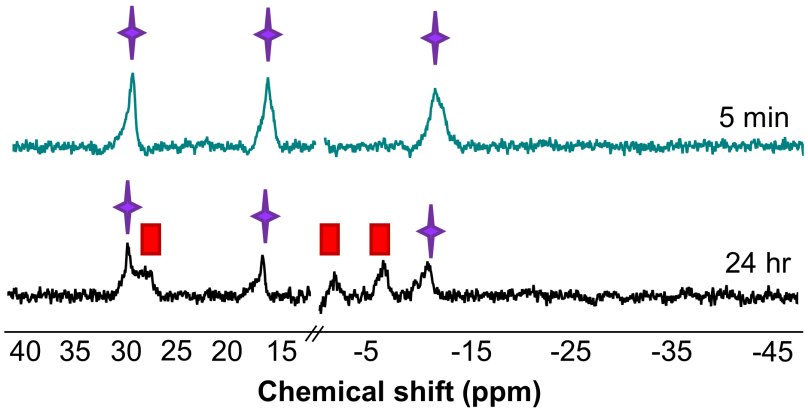

Figure S9. ^{1}H NMR spectra in the paramagnetic region of reaction of Hydz with one equivalent of **[$V_6O_6(MeCN)]^0$** at 21°C for after 5 min (top, teal) and 1 day (bottom, black) recorded in THF-d_8 at 294 K. Purple stars indicate starting material **[$V_6O_6(MeCN)]^0$** and red squares indicate the formation of **[$V_6O_5(MeCN)(OH_2)]^0$**.

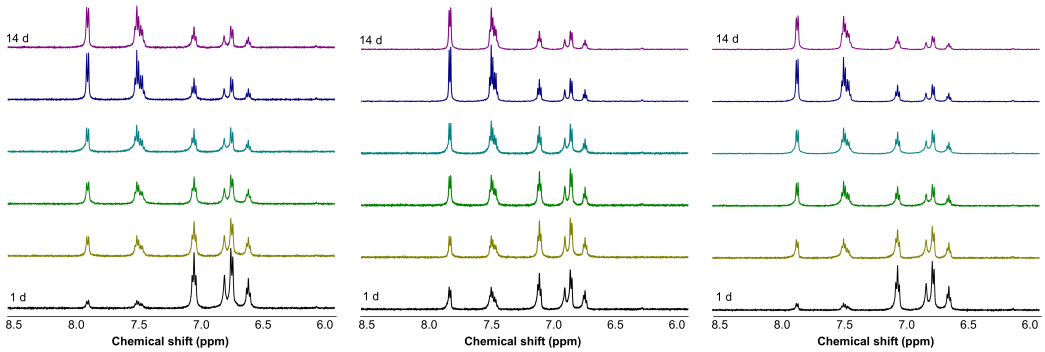

Figure S10. ^{1}H NMR spectra in the diamagnetic region of reaction of Hydz with one equivalent of **[V_6O_6(MeCN)]^0** at 294 K, over 14 days in THF-d_8, trial A-C (left to right). Growth of oxidized organic reagent (Azo) is seen at 7.5 and 7.9 ppm.

Table S4. $BDFE_{adj}$ calculated for **[V_6O_5(MeCN)(OH_2)]^0** from equilibrium reactions described in Figure S9, using the equation outlined in the Experimental section in the main text.

	Hydrazobenzene					Azobenzene[b]					
	7.06 ppm (4 H)		6.77 ppm (6 H)		Avg.	7.92 ppm (4 H)		7.52 ppm (6 H)		Avg.	
Trial	Integral	Relative Conc.[a]	Integral	Relative Conc.[a]	Conc.	Integral	Relative Conc.[a]	Integral	Relative Conc.[a]	Conc.	$BDFE_{adj}$ (kcal/mol)
A	0.52	0.13	0.70	0.116	0.125	1	0.25	1.55	0.258	0.254	60.6
B	0.50	0.125	0.63	0.105	0.115	1	0.25	1.55	0.258	0.254	60.7
C	0.45	0.113	0.54	0.09	0.102	1	0.25	1.58	0.263	0.256	60.7
										Avg.	60.7
										Std. Dev.	0.1

[a] Relative concentration of either hydrazobenzene or azobenzene was determined by dividing the integral by the number of protons a given signal(s) corresponds with.

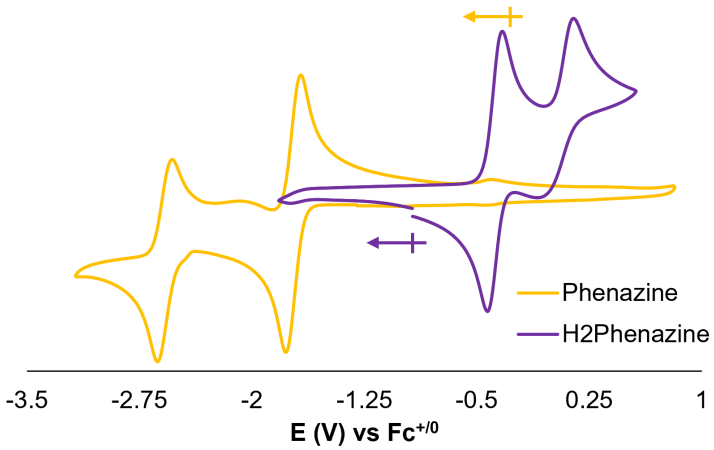

Figure S11. CV of 2 mM H_2Phen (purple) and Phen (orange) collected at 100 mVs^{-1} in THF with 200 mM [^{n}Bu$_4$N][PF_6] supporting electrolyte.

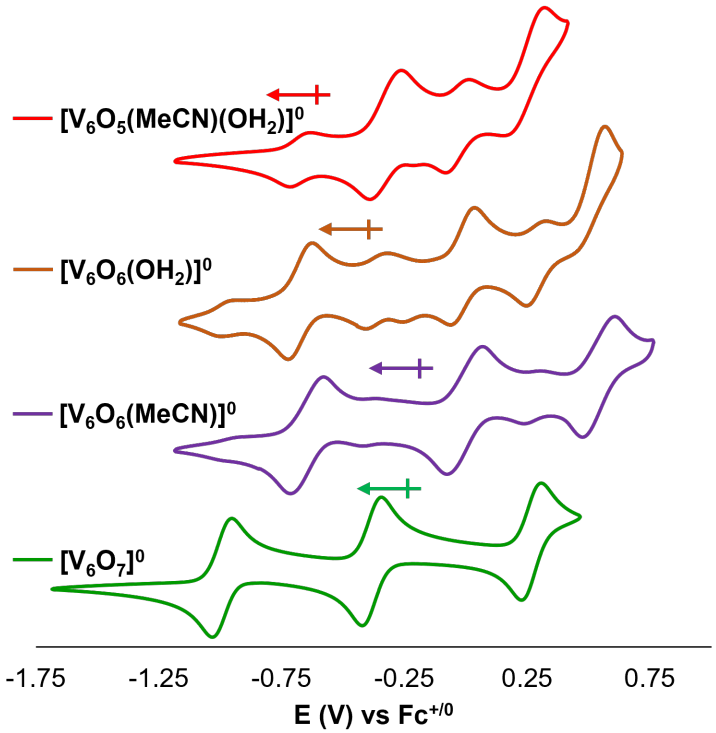

Figure S12. CV of 1 mM $[V_6O_7]^0$ (green), $[V_6O_6(MeCN)]^0$ (purple), $[V_6O_6(OH_2)]^0$ (orange), and $[V_6O_5(MeCN)(OH_2)]^0$ (red) collected at 100 mVs^{-1} in THF with 200 mM $[^nBu_4N][PF_6]$ supporting electrolyte versus $Fc^{+/0}$. Due to electrochemical instability of the O-atom deficient species, some features of the corresponding oxidized complex are observed on the CV timescale.

Table S5. Redox potentials of $[V_6O_7]^0$, $[V_6O_6(MeCN)]^0$, $[V_6O_6(OH_2)]^0$, $[V_6O_5(MeCN)(OH_2)]^0$, Phen, and H_2Phen from CVs in Figure S12 (vs $Fc^{+/0}$). The position of the open circuit voltage is denoted by the red border lines

$[V_6O_7]^0$	$[V_6O_6(MeCN)]^0$	$[V_6O_6(OH_2)]^0$	$[V_6O_5(MeCN)(OH_2)]^0$	Phen	H_2Phen
-0.994	-0.646	-0.674	-0.325	-2.57	-0.387
-0.385	-0.0197	-0.0231	0.222	-1.72	0.0240
0.267	0.523	0.467	-	-	-

Table S6. Determination of the average pK_a's of H_2Phen, "$[V_6O_6(OH_2)]^{2+}$", and "$[V_6O_5(MeCN)(OH_2)]^{2+}$" in THF using the Bordwell Equation.

Compound	BDFE (kcal mol^{-1})	E^0 [a] (V, vs $Fc^{+/0}$)	E^0 (avg) (V, vs $Fc^{+/0}$)	C_G (kcal mol^{-1})	pK_a
H_2Phen	59.2	-1.72, -2.57	-2.15	59.9	35.6
"$[V_6O_5(MeCN)(OH_2)]^{2+}$"	60.7	-0.646, -0.0197	-0.0514	59.9	1.45
"$[V_6O_6(OH_2)]^{2+}$"	62.3	-0.0231, 0.467	0.222	59.9	-1.98

[a] $1e^-$ redox potentials of respective species. For H_2Phen, the reduction events of Phen were used. For cluster species, the oxidation potentials of the **$[V_6O_5(MeCN)(OH_2)]^0$** and **$[V_6O_6(OH_2)]^0$** were used.

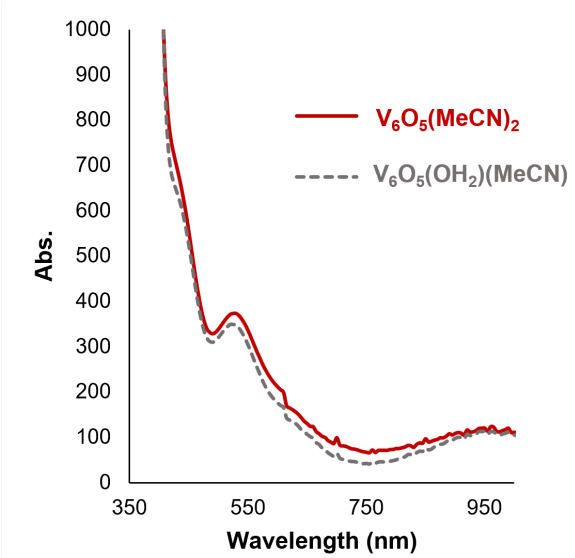

Figure S13. Electronic absorption spectrum of **$[V_6O_5(OH_2)(MeCN)]^0$** , grey dotted trace and **$[V_6O_5(MeCN)_2]^0$**, red trace, recorded at 21 °C in THF.

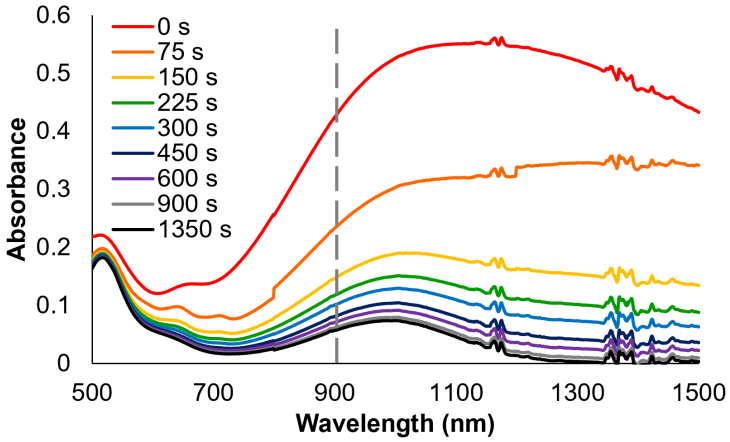

Figure S14. UV-Vis NIR of **$[V_6O_6(MeCN)]^0$** (0.83 mM)+ 1 eq H_2Phen (0.83 mM) over time at 238 K in MeCN.

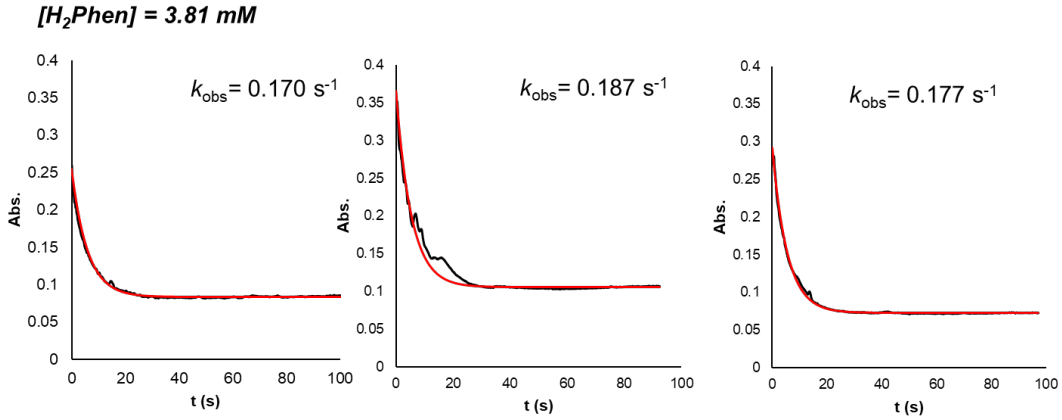

Figure S15. Plot of absorbance at 900 nm over time for reactions between **$[V_6O_6(MeCN)]^0$** (0.75 mM) and excess H_2Phen (3.81 mM) under pseudo-first order conditions recorded in CH_3CN at 258 K, with raw data (black) and a fit curve (red). Concentration of H_2Phen for each reaction is noted, alongside the fit-derived k_{obs}. Triplicate data sets are reported.

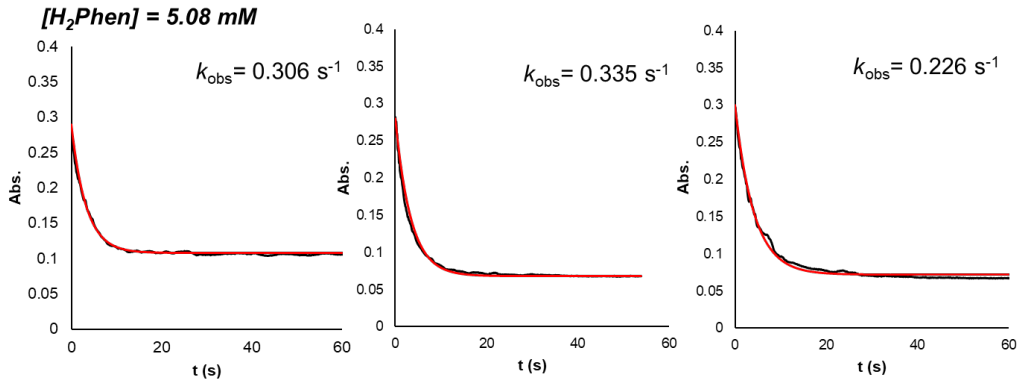

Figure S16. Plot of absorbance at 900 nm over time for reactions between **$[V_6O_6(MeCN)]^0$** (0.75 mM) and excess H_2Phen (5.08 mM) under pseudo-first order conditions recorded in CH_3CN at 258 K, with raw data (black) and a fit curve (red). Concentration of H_2Phen for each reaction is noted, alongside the fit-derived k_{obs}. Triplicate data sets are reported.

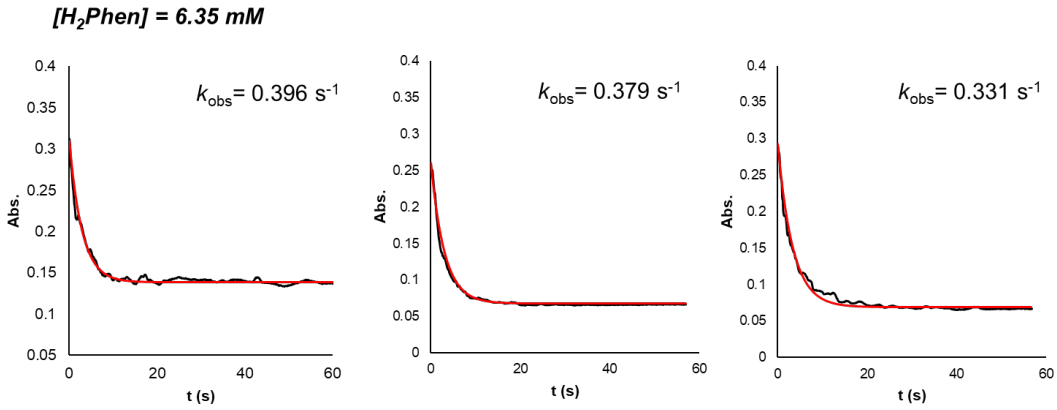

Figure S17. Plot of absorbance at 900 nm over time for reactions between **$[V_6O_6(MeCN)]^0$** (0.75 mM) and excess H_2Phen (6.35 mM) under pseudo-first order conditions recorded in CH_3CN at 258 K, with raw data (black) and a fit curve (red). Concentration of H_2Phen for each reaction is noted, alongside the fit-derived k_{obs}. Triplicate data sets are reported.

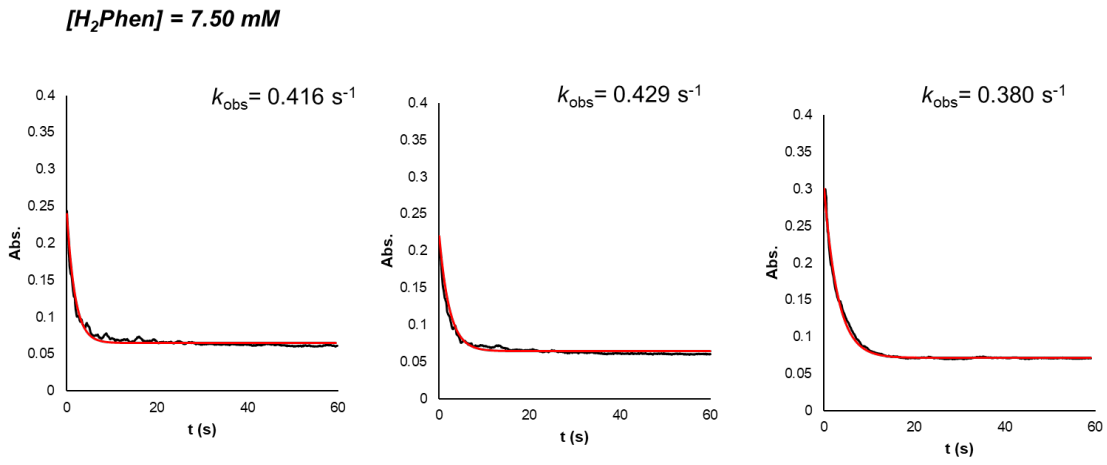

Figure S18. Plot of absorbance at 900 nm over time for reactions between $[V_6O_6(MeCN)]^0$ (0.75 mM) and excess H_2Phen (7.50 mM) under pseudo-first order conditions recorded in CH_3CN at 258 K, with raw data (black) and a fit curve (red). Concentration of H_2Phen for each reaction is noted, alongside the fit-derived k_{obs}. Triplicate data sets reported.

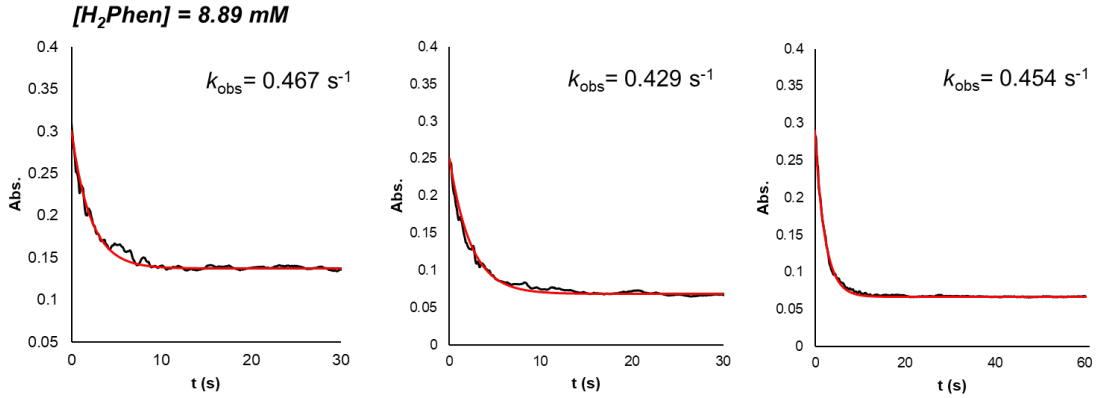

Figure S19. Plot of absorbance at 900 nm over time for reactions between $[V_6O_6(MeCN)]^0$ (0.75 mM) and excess H_2Phen (8.89 mM) under pseudo-first order conditions recorded in CH_3CN at 258 K, with raw data (black) and a fit curve (red). The fit-derived k_{obs} is noted. Triplicate data sets are reported.

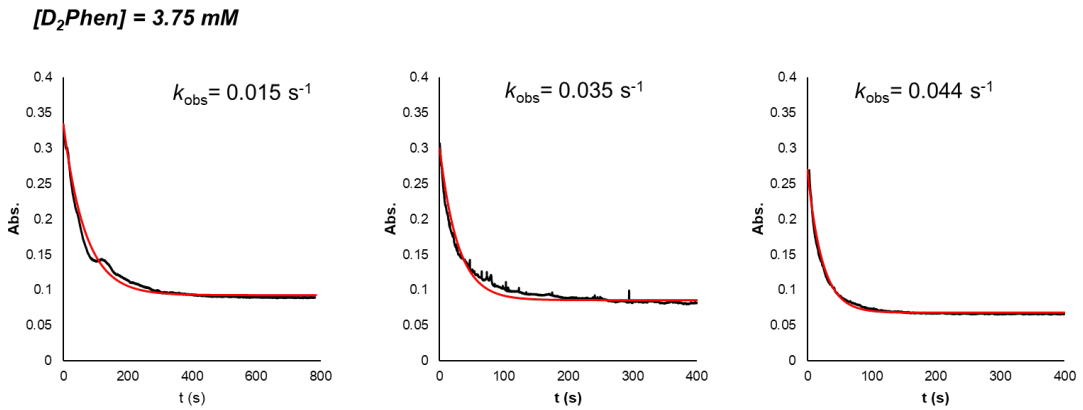

Figure S20. Plots of absorbance at 900 nm over time for reactions between $[V_6O_6(MeCN)]^0$ (0.75 mM) and excess D_2Phen (3.75 mM) under pseudo-first order conditions recorded in CH_3CN at 258 K, with raw data (black) and a fit curve (red). The fit-derived k_{obs} is noted. Triplicate data sets are reported.

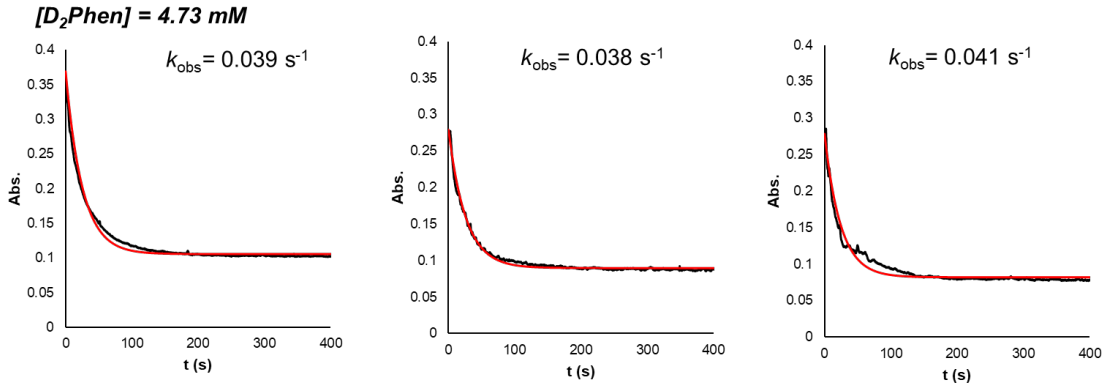

Figure S21. Plots of absorbance at 900 nm over time for reactions between $[V_6O_6(MeCN)]^0$ (0.75 mM) and excess D_2Phen (4.73 mM) under pseudo-first order conditions recorded in CH_3CN at 258 K, with raw data (black) and a fit curve (red). The fit-derived k_{obs}. Triplicate data sets are reported.

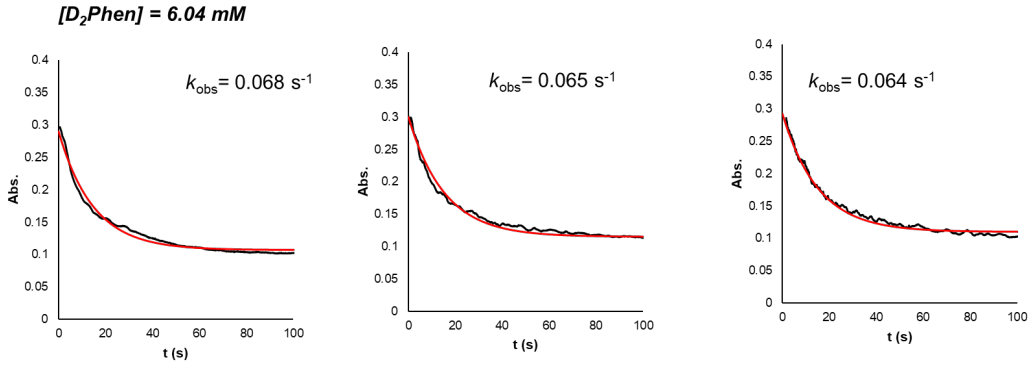

Figure S22. Plots of absorbance at 900 nm over time for reactions between **$[V_6O_6(MeCN)]^0$** (0.75 mM) and excess D_2Phen (6.04 mM) under pseudo-first order conditions recorded in CH_3CN at 258 K, with raw data (black) and a fit curve (red). Concentration of D_2Phen for each reaction is noted, alongside the fit-derived k_{obs}.

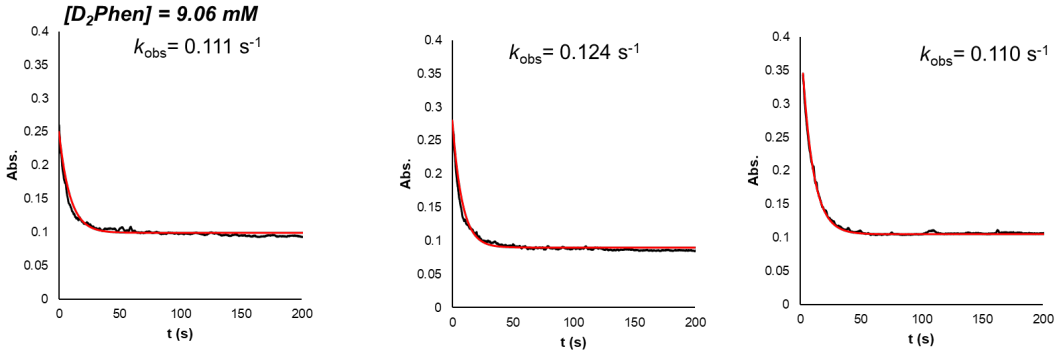

Figure S23. Plots of absorbance at 900 nm over time for reactions between **$[V_6O_6(MeCN)]^0$** (0.75 mM) and excess D_2Phen (9.06 mM) under pseudo-first order conditions recorded in CH_3CN at 15 °C, with raw data (black) and a fit curve (red). The fit-derived k_{obs} is noted. Triplicate data sets are reported.

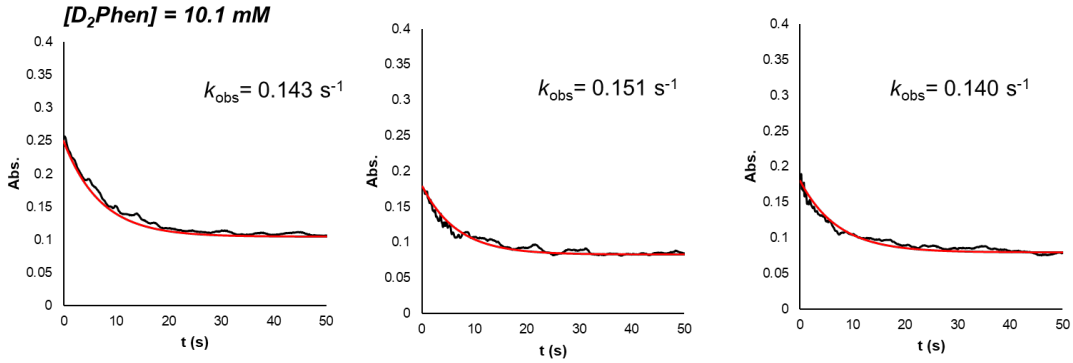

Figure S24. Plots of absorbance at 900 nm over time for reactions between **$[V_6O_6(MeCN)]^0$** (0.75 mM) and excess D_2Phen (10.1 mM) under pseudo-first order conditions recorded in CH_3CN at 258 K, with raw data (red) and a fit curve (black). The fit-derived k_{obs} is noted. Triplicate data sets reported.

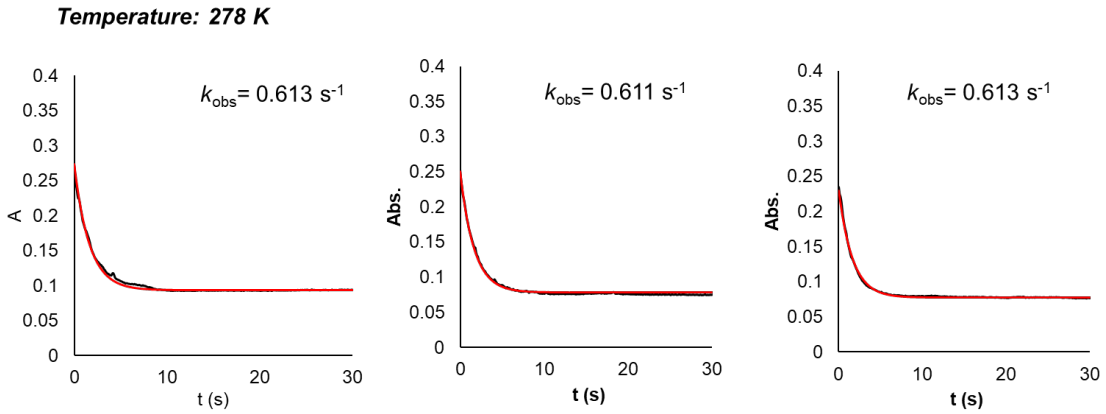

Figure S25. Plots of absorbance at 900 nm over time for reactions between **$[V_6O_6(MeCN)]^0$** (0.75 mM) and H_2Phen (7.26 mM) recorded in CH_3CN at 278 K, with raw data (black) and a fit curve (red), providing k_{obs}. Triplicate data sets are reported.

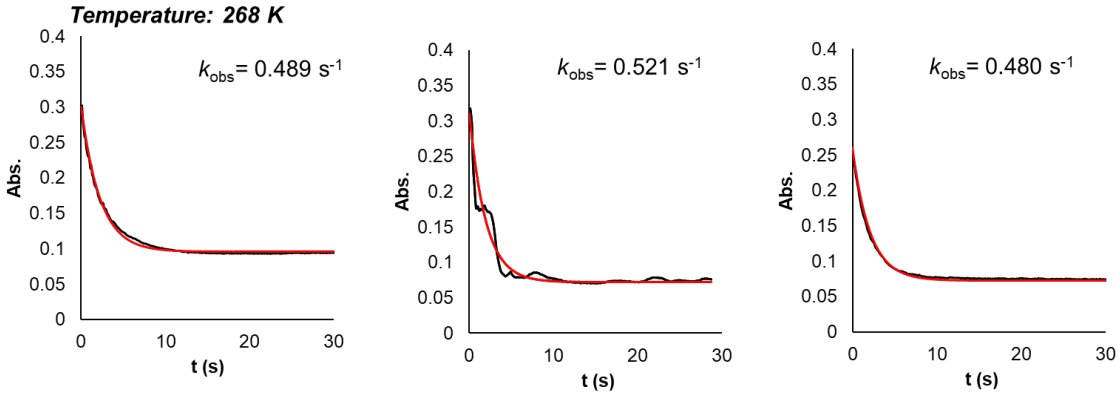

Figure S26. Plots of absorbance at 900 nm over time for reactions between **$[V_6O_6(MeCN)]^0$** (0.75 mM) and H_2Phen (7.26 mM) recorded in CH_3CN at 268 K, with raw data (black) and a fit curve (red), providing k_{obs}. Triplicate data sets are reported.

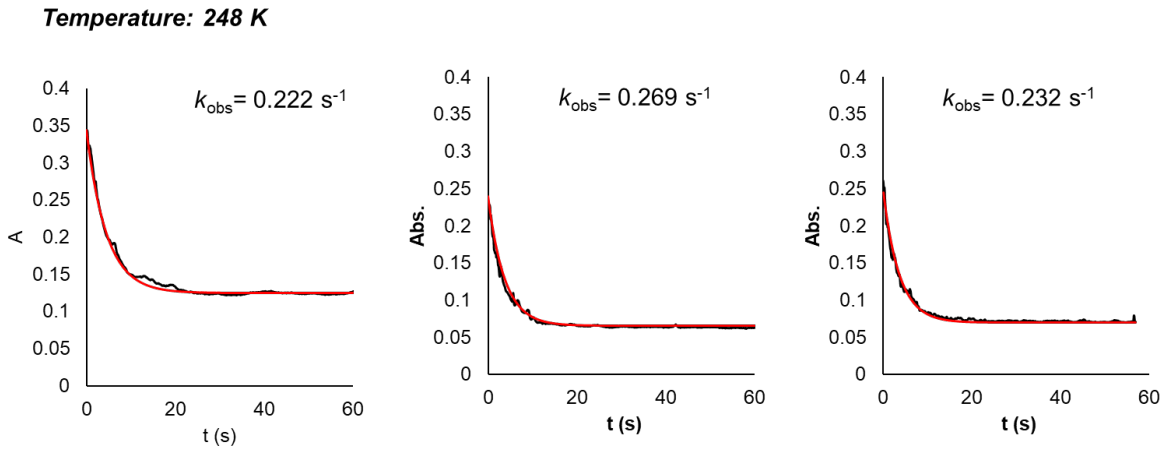

Figure S27. Plots of absorbance at 900 nm over time for reactions between **$[V_6O_6(MeCN)]^0$** (0.75 mM) and H_2Phen (7.26 mM) recorded in CH_3CN at 248 K, with raw data (black) and a fit curve (red), providing k_{obs}. Triplicate data sets are reported.

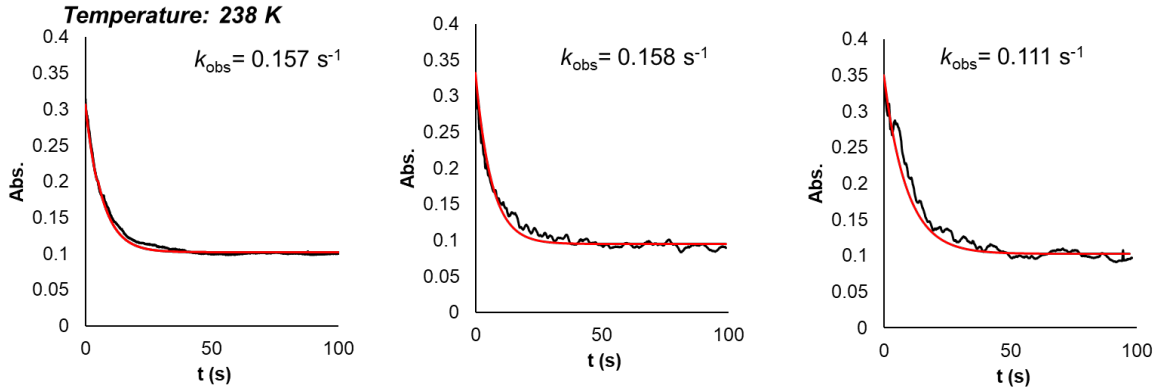

Figure S28. Plots of absorbance at 900 nm over time for reactions between **$[V_6O_6(MeCN)]^0$** (0.75 mM) and H_2Phen (7.26 mM) recorded in CH_3CN at 238 K, with raw data (black) and a fit curve (red), providing k_{obs} and k_{exp}.

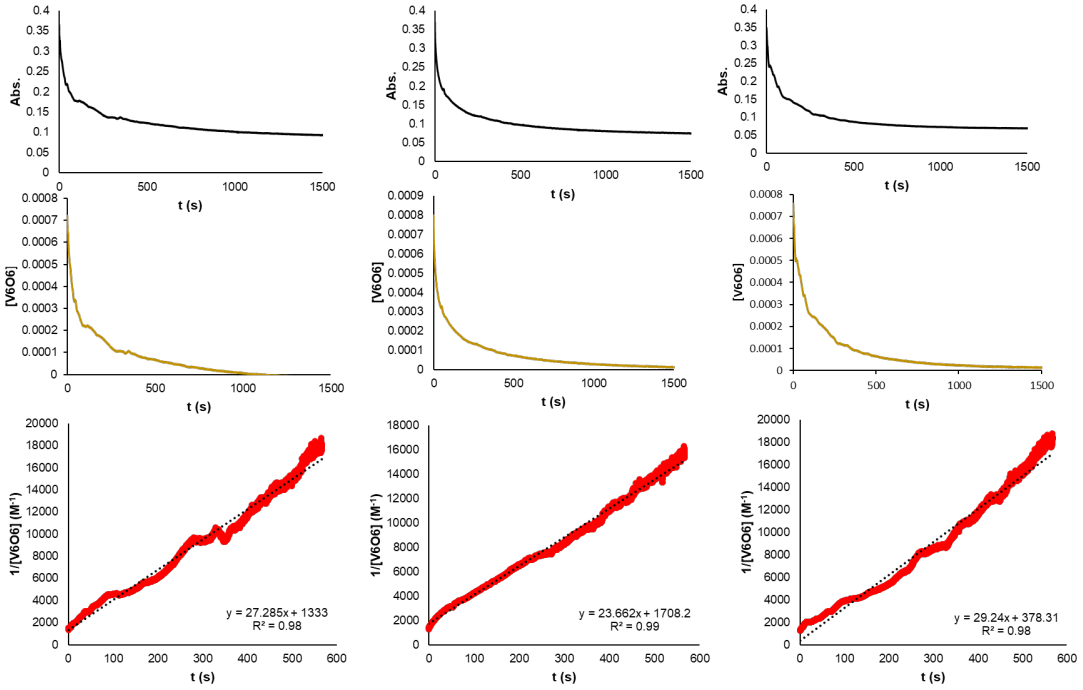

Figure S29. **$V_6O_6(MeCN)$** (0.75 mM) + 1 eq H_2Phen (0.75 mM) in MeCN, over 30 minutes at 258 K. Exponential decay of **$V_6O_6(MeCN)$** is monitored at 900 nm to least 3 half-lives, (top, black trace). Concentration of **$V_6O_6(MeCN)$** converted from absorbance using the following equations:$[\mathbf{V_6O_6}]_t=[\mathbf{V_6O_6}]_0-[\mathbf{V_6O_5}]_t$ and $[\mathbf{V_6O_5}]_t=(A_0-A_t)/(\varepsilon_{\mathbf{V6O6}}-\varepsilon_{\mathbf{V6O5}})$,[2] where @ 900 nm $\varepsilon_{\mathbf{V6O6}}$ = 415 M^{-1} cm^{-1}, $\varepsilon_{\mathbf{V6O5}}$ = 98 M^{-1} cm^{-1}, (middle, yellow trace). Plot of 1/**$[V_6O_6(MeCN)]$** vs t (bottom, red trace. Black dotted line indicates linear fit). Diving the slope by the # of V=O and H-atoms transferred gets a second order k_{PCET}= 3.5 ± 0.1 M^{-1} s^{-1}. Data sets reported in triplicate.

References

1. B. E. Petel, A. A. Fertig, M. L. Maiola, W. W. Brennessel and E. M. Matson, *Inorganic Chemistry*, 2019, **58**, 10462-10471.
2. X. Lu, X. Li, Y. Lee, Y. Jang, M. S. Seo, S. Hong, K. Cho, S. Fukuzumi and W. Nam, *Journal of the American Chemical Society* 2020 **142**, 3891-3904.